Letter

Gouy phase-matched angular and radial mode conversion in four-wave mixing

Rachel F. Offer,* Andrew Daffurn, Erling Riis, Paul F. Griffin, and Aidan S. Arnold†
Department of Physics, SUPA, University of Strathclyde, Glasgow G4 0NG, United Kingdom

Sonja Franke-Arnold
School of Physics and Astronomy, SUPA, University of Glasgow, Glasgow G12 8QQ, United Kingdom

(Received 27 July 2020; accepted 8 February 2021; published 25 February 2021)

Studying the conversion between transverse light modes via four-wave mixing in a heated rubidium vapor, we demonstrate and explain a transfer between azimuthal and radial mode numbers. They relate to orthogonal modal dimensions, which one would not normally expect to interact. While angular momentum conservation in this nonlinear process dictates the selection rules for the angular mode number, the role of the radial mode number is more esoteric. We demonstrate systematically that the Gouy phase is the key to understanding this conversion, leading to strikingly different conversion behavior in the thick- and thin-medium regimes. Our experimental investigation of the transition between these regimes bridges the gap between previous experiments in atomic thick media and work in nonlinear crystals. Our work sets a clear starting point to explore the thick-medium regime, allowing efficient radial-to-azimuthal and radial-to-radial mode conversion.

DOI: 10.1103/PhysRevA.103.L021502

Laguerre-Gauss (LG) beams and their corresponding orbital angular momentum (OAM) have been a burgeoning research area since their association in 1992 [1]. They have applications in microfabrication [2], entanglement protocols [3,4], and multiplexing in classical as well as quantum communication systems [5–7] and are summarized in a plethora of reviews and road maps [8–11]. These studies have been devoted almost exclusively to the study of the azimuthal mode index ℓ of the LG modes, while the radial index p remains largely unexplored.

The azimuthal mode number has a simple geometrical interpretation: beams with an azimuthal phase winding $\exp(i\ell\theta)$ carry an OAM of $\ell\hbar$ per photon, a quantum interpretation of the Fourier conjugate relation between angle and angular momentum. Understanding the radial mode number, however, is less intuitive, as the observed p-mode decomposition of a beam depends on the chosen fundamental waist, and a generating function is not readily identified [12]. Nevertheless, various strategies have been devised to assess radial modes [13–18], and several recent publications highlight their role in detailed quantum investigations [19–24].

In nonlinear processes, including spontaneous parametric down-conversion (SPDC), second-harmonic generation (SHG), and four-wave mixing (FWM), the full three-dimensional (3D) overlap of all participating modes determines the efficiency of mode conversion [25,26]. The transverse overlap, specifically the integration over the azimuthal angle, is sufficient to define phase matching and hence angular momentum conservation in nonlinear crystals [26–29] and in atomic vapors [30–33]. In extended media, however, the relative Gouy phase of the involved modes becomes important [34–39].

Here, we perform and analyze FWM of arbitrary LG modes in an atomic vapor, reaching, with the same experimental setup, the equivalent of both the thin and thick crystal limits, which are characterized by strikingly different behaviors. This allows us to investigate nonlinear interaction regions beyond the Rayleigh range, a regime not usually accessed in crystal-based SPDC and SHG. We explain the difference in behavior by a phase-matching condition—Gouy phase matching—which gains importance as the interaction length reaches and exceeds the Rayleigh range. In the thick-medium regime this restricts the number of modes generated, allowing us to demonstrate clean azimuthal-to-radial and radial-to-radial mode conversion.

Conversion between modes of different azimuthal mode numbers has been associated with angular momentum conservation [28,29]; however, there exists no obvious conservation law that would lead to a conversion between radial and azimuthal mode numbers. Coupling between orthogonal mode indices can result from symmetry breaking via dissipation or boundary conditions and has been observed on platforms as diverse as optical fibers and waveguides, acoustics, stellar interiors, and supercooled liquids. These effects are usually seen as detrimental and lead to a loss of purity. This contrasts with our observations for mode conversion via four-wave mixing in the thick-medium regime experiments, where Gouy phase matching facilitates efficient and controlled mode manipulation.

Before discussing the experiments we briefly outline our theoretical model. We predict FWM efficiency by evaluating the mode-overlap integral of all involved complex electric

*rachel.offer@adelaide.edu.au
†aidan.arnold@strath.ac.uk

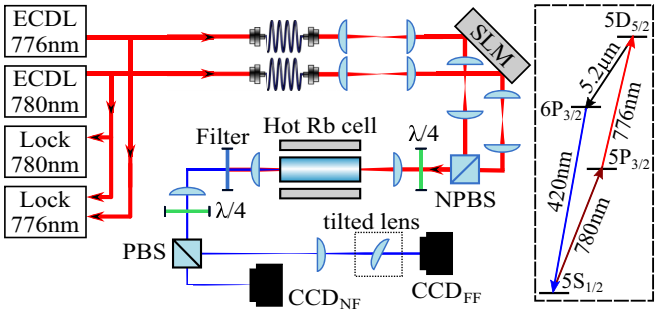

FIG. 1. Experimental setup and level scheme. Fiber-coupled 780- and 776-nm pump beams from extended-cavity diode lasers (ECDLs) are independently shaped on an SLM (incidence angle exaggerated) into pure LG_p^ℓ modes. They are relayed through beam telescopes, combined on a nonpolarizing beam splitter (NPBS), co-circularly polarized with a quarter-wave plate ($\lambda/4$), and focused into a hot rubidium vapor cell. A filter isolates the blue light generated by FWM. The near and far fields from the Rb cell are imaged on cameras $\mathrm{CCD_{NF}}$ and $\mathrm{CCD_{FF}}$ and analyzed using a removable tilted lens.

fields, following Refs. [30,33,40],

$$\int_0^{2\pi} d\theta \int_0^{\infty} r\,dr \int_{-L/2}^{L/2} dz\, u_{780}\, u_{776}\, u_{\mathrm{IR}}^*\, u_{\mathrm{B}}^*, \tag{1}$$

where the subscripts denote the input electric fields at wavelengths of 780 and 776 nm and the generated fields at 5233 nm [infrared (IR)] and 420 nm [blue (B)]; Fig. 1, inset. We use cylindrical polar coordinates and assume that the pump fields are focused at the center of a vapor cell, with length L.

Any paraxial beam $u(r,z,\theta)$ can be decomposed in the LG_p^ℓ basis (for more details, see Supplemental Material [41], Sec. S1),

$$\mathrm{LG}_p^\ell(r,z,\theta) = A_p^{|\ell|}(r,z)\; e^{i\ell\theta}\; e^{i\Phi_{\mathrm{G}}(z)}, \tag{2}$$

where $A_p^{|\ell|}$ is a complex amplitude and the azimuthal phase is $\ell\theta$. The Gouy phase

$$\Phi_{\mathrm{G}}(z) = -(1+2p+|l|)\arctan(z/z_{\mathrm{R}}) \tag{3}$$

describes the phase evolution of a mode propagating through a focus, with $z_{\mathrm{R}} = \pi w_0^2/\lambda$ denoting the Rayleigh range for a beam waist w_0. The relative Gouy phase between modes with different mode numbers $N_p^\ell = 1+2p+|l|$ crucially affects mode conversion.

The azimuthal integral of Eq. (1) leads to the condition that OAM must be conserved,

$$\ell_{780} + \ell_{776} = \ell_{\mathrm{IR}} + \ell_{\mathrm{B}}. \tag{4}$$

We assume the Boyd criterion [42] holds; that is, the waists of the generated fields yield the same Rayleigh range as the pump fields. Evaluating the axial integral introduces a dependence on the relative Gouy phase of the modes. Fields with differing mode numbers N_p^ℓ slip out of phase as they propagate through the cell, leading to a reduced FWM efficiency.

In the extreme thick-crystal limit, where $z_{\mathrm{R}} \ll L$, the Gouy phase of each field changes by $N_p^\ell\pi$ as it propagates through the cell. For the beams to remain (Gouy) phase matched, the total mode order must therefore also be conserved, leading to the condition

$$\left(N_p^\ell\right)_{780} + \left(N_p^\ell\right)_{776} = \left(N_p^\ell\right)_{\mathrm{IR}} + \left(N_p^\ell\right)_{\mathrm{B}}. \tag{5}$$

Only mode combinations that obey Eqs. (4) and (5) contribute to FWM. This is strictly true only in the thick-crystal limit. For any extended medium, however, the evaluation of the axial mode-overlap integral results in a decreased efficiency of mode combinations with unmatched Gouy phases.

In our experiment the 420-nm light is generated as a superposition of one or more modes, depending on the ratio of cell length to Rayleigh range. The presence of multiple coherent modes becomes apparent from the spatial variation of the light's intensity on propagation: individual LG modes and their incoherent mixtures have a self-similar intensity profile upon propagation, with radial size scaling as the beam radius. Interference between coherent superpositions with differing mode numbers and hence Gouy phases, however, results in a modulation of the intensity profile [43–47], with notable differences between near- and far-field profiles. This behavior serves as a simple way of determining mode population and coherence experimentally. We additionally analyze the modal decomposition in a single plane using a tilted-lens technique [48].

Our FWM scheme (Fig. 1) utilizes the extreme single-pass efficiencies found even at milliwatt powers in the highly nondegenerate diamond atomic-level system of alkali-metal vapors [49–55]. Near-infrared external cavity diode lasers [56] at 780- and 776-nm pump the input transitions of an ^{85}Rb diamond level system (inset Fig. 1), with laser and lock details given in Sec. S2 of the Supplemental Material [41]. FWM, seeded by initial spontaneous emission, generates coherent light beams at 5.2 μm and 420 nm, in the cascade back to the ground state. We use two separate regions of the same spatial light modulator (SLM) to independently shape the complex amplitudes of the 780- and 776-nm pump laser beams, generating high-purity LG modes [33,57].

Our experimental setup permits us to vary smoothly between a "thick" medium ($z_{\mathrm{R}} \ll L$) and a "thin" medium ($z_{\mathrm{R}} \gg L$), allowing us to reconcile the respective selection rules for mode conversion in FWM in the different regimes. We adjust the beam waist w_0 of the pump lasers by using different telescopic optics, thereby changing the Rayleigh length z_{R} relative to the fixed cell length of $L = 25$ mm.

We first investigate the conversion of pump modes with opposite angular mode indices to FWM light with a nonzero radial mode index and examine the behavior in the thick- and thin-medium regimes. Specifically, we demonstrate FWM for the case of $u_{780} = \mathrm{LG}_0^1$ and $u_{776} = \mathrm{LG}_0^{-1}$ pump light. Figures 2(a) and 2(b) depict the corresponding experimental beam profiles observed in the near and far fields as well as through a tilted lens [48] to visualize their angular mode number ℓ, where the number of lobes is given by $|\ell|+1$ and the tilt corresponds to the sign of the OAM.

The 5.2-μm infrared light is currently absorbed by our glass cell but could be readily detected with a sapphire cell. If the unobserved IR beam is dominantly generated in the mode $u_{\mathrm{IR}} = \mathrm{LG}_0^0$, OAM conservation [Eq. (4)] dictates that $\ell_{\mathrm{B}} = 0$. The only solution also satisfying Gouy phase matching [Eq. (5)] is $p_{\mathrm{B}} = 1$; thus, in the thick-crystal limit we

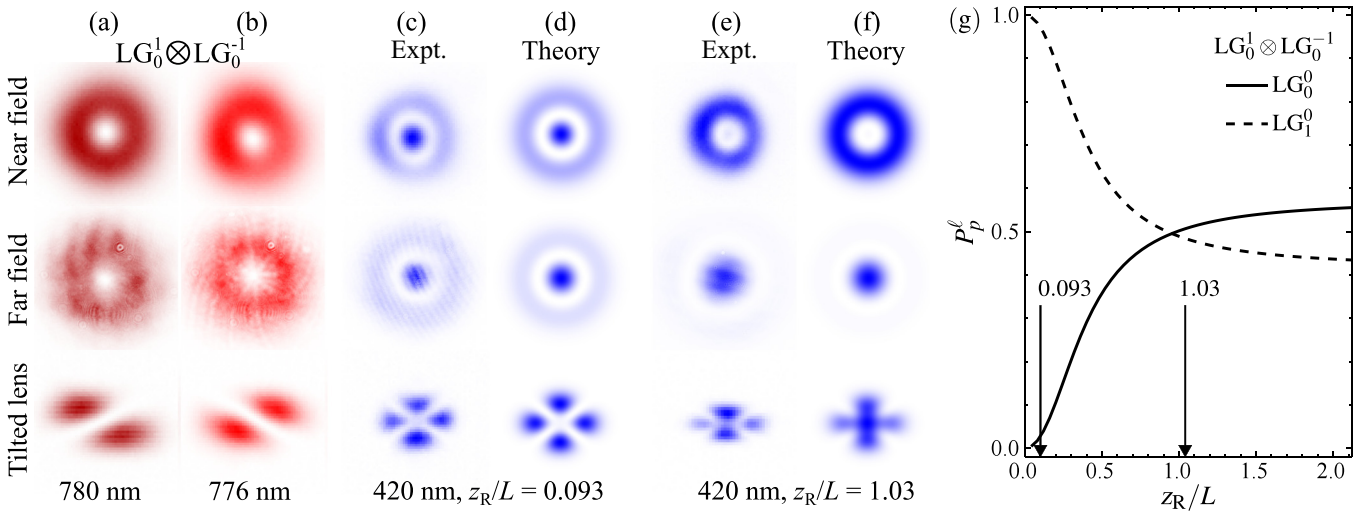

FIG. 2. FWM for pump modes with opposite ℓ: (a) LG_0^1 at 780 nm and (b) LG_0^{-1} at 776 nm. For a thick medium, we observe (c) 420-nm light in an almost pure LG_1^0 mode, in agreement with (d) our model. For a thin medium (e) the experimental and (f) predicted light is a coherent superposition of LG_0^0 and LG_1^0. Each image triplet in (a)–(f) corresponds to the near- field (top), far-field (middle), and tilted-lens (bottom) beam intensity. Individual images are peak normalized, and color saturation corresponds linearly to light intensity. In (g) we simulate the impact of the medium thickness on the mode purity of the generated light, with $LG_0^1 \otimes LG_1^{-1}$ input.

expect $u_B = LG_1^0$. This is a counterintuitive result, as it allows the generation of light with on-axis intensity from modes with a central vortex with associated null intensity.

The resulting FWM light at 420 nm is shown for the thick- and thin-medium limits in Figs. 2(c) and 2(e), respectively. The thick (thin) regime is realized by setting the pump waist to $w_0 = 24\,\mu m$ (80 μm), corresponding to an "inverse-thickness" parameter $z_R/L = 0.093$ (1.03). In the thick-medium regime [Fig. 2(c)], the LG_0^1 and LG_0^{-1} pump light generates an almost pure blue LG_1^0 mode, easily recognized by its bright central spot and surrounding ring, separated by a ring of zero intensity. Moreover, the beam is self-similar in both the near (top image) and far (middle) fields, illustrating its single-mode nature. The tilted-lens image (bottom) corroborates this interpretation, with $\ell_B = 0$ as determined by the difference between the number of lobes in the diagonal and antidiagonal directions and $p_B = 1$ determined by the minimum of these numbers minus 1. These results agree with a simulation of the beam profiles based on evaluating the mode-overlap integral (1), shown in Fig. 2(d).

The situation is markedly different in the thin-medium regime, where Gouy phase matching is relaxed, while OAM conservation holds strictly. Evaluating the mode-overlap integral shows that the beam is generated in an almost equal superposition of LG_0^0 and LG_1^0. This is confirmed by our observations and simulations in Figs. 2(e) and 2(f). The near field is a lone intensity ring reminiscent of the pump-field overlap, and the far field is dominated by a central spot. This arises because the differing mode numbers, $N_0^0 = 1$ and $N_1^0 = 3$, modify the modal interference from the near to the far field, yielding a π Gouy phase shift. Moreover, the tilted-lens image confirms that $\ell = 0$, and we no longer have a single mode, as the spots have no clear nodal delineation. Further experimental results for $0.49 \leqslant z_R/L \leqslant 1.03$ are included in Fig. S1 in the Supplemental Material [41].

We support our observations by evaluating the 3D overlap integral of Eq. (1) as a function of medium thickness, identifying the relative efficiency of all possible output mode combinations $u_B u_{IR}$. We note that this simple model does not include the effect of the atoms on the optical propagation, e.g., via absorption, Kerr lensing, or stimulated processes. In the thick-medium regime this results in the generation of all mode pairs obeying OAM conservation and Gouy phase matching, i.e., $LG_1^0\,LG_0^0$, $LG_0^0\,LG_1^0$, $LG_0^1\,LG_0^{-1}$, $LG_0^{-1}\,LG_0^1$ in the ratio 0.36:0.36:0.13:0.13, and negligible power in a variety of additional modes, with more modes becoming viable for thinner media.

Interestingly, our simulations agree best with experimental observations if we constrain the infrared to LG_0^0, regardless of medium thickness. In our previous work with $LG_{p=0}^{\ell>0}$ input modes [30,33] this arose naturally for low ℓ as the midinfrared light has a larger waist from the Boyd criterion. We note that the situation for modes with $p > 0$ is more complex as their size no longer scales as a direct function of the mode index. Instead, we expect that the selection of the infrared LG_0^0 mode is a consequence of the full propagation dynamics. Figure 2(g) shows the predicted mode decomposition assuming $u_{IR} = LG_0^0$. This assumption is applied to all theoretical results in this work.

We compare our work with earlier investigations on mode conversion. While we show results in the thick- and thin-medium regimes with $z_R/L \simeq 0.1$ and 1, respectively, experiments performed using SHG [34,37,38] appear to all have $z_R/L \geqslant 10$, at least an order of magnitude thinner than demonstrated here. The observed second-harmonic beam profile in these publications agrees with our assumption that in this thin regime total mode order conservation is relaxed, so that a spectrum of radial modes can be generated. According to our model, the most drastic changes to mode conversion happen for $z_R/L \leqslant 2$, before reaching an asymptotic limit.

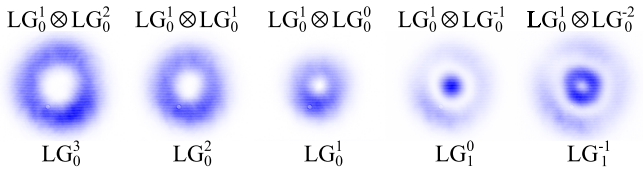

FIG. 3. Thick-medium blue FWM light arising from mixing 780-nm LG_0^1 with 776-nm $LG_0^{2,1,0,-1,-2}$ pump modes (left to right), with a transition from $p = 0$ to $p = 1$ when ℓ_{776} becomes negative (see Fig. 2).

Additionally, in a FWM system similar to our own, but with fixed $z_R \sim L$ [31], the 420-nm light was observed as a ring-shaped intensity profile with slight on-axis intensity, indicative of partial conversion to radial modes.

For $p = 0$ pump modes with the same intensity profile but equal OAM of $\ell = 1$, OAM conservation and Gouy phase matching restrict the generated blue light to an almost pure LG_0^2 mode, regardless of medium thickness (Supplemental Material [41], Fig. S2). In this situation, as well as similar experiments with pump modes of equal-handed OAM, no conversion between the angular and radial mode indices occurs. Investigating the onset of angular-to-radial mode conversion, we find that for $p = 0$ pump beams, the blue light features a radial mode index of $p_B = (|\ell_{780}| + |\ell_{776}| - |\ell_{780} + \ell_{776}|)/2$ when working in a thick medium where Gouy phase matching applies (and for $u_{IR} = LG_0^0$). We demonstrate this for input modes $u_{780} \otimes u_{776} = LG_0^1 \otimes LG_0^{\ell_{776}}$, with $\ell_{776} \in \{-2, -1, 0, 1, 2\}$, which transform cleanly into a blue LG mode, where $\ell_B = 1 + \ell_{776}$ and $p_B = 0$ for $\ell_{776} \geqslant 0$ and $p_B = 1$ for $\ell_{776} < 0$ (Fig. 3 and Supplemental Material [41], Fig. S3).

In the following we extend our investigation to the mode conversion of pump beams with $p \neq 0$. In Fig. 4 we show that pumping with $u_{780} = u_{776} = LG_1^1$ generates a clean LG_2^2 blue output mode if operating in the thick-medium regime. For a thin medium, a coherent superposition of modes with different mode orders is generated, leading to a changing intensity profile between the near and far fields. Here our simple

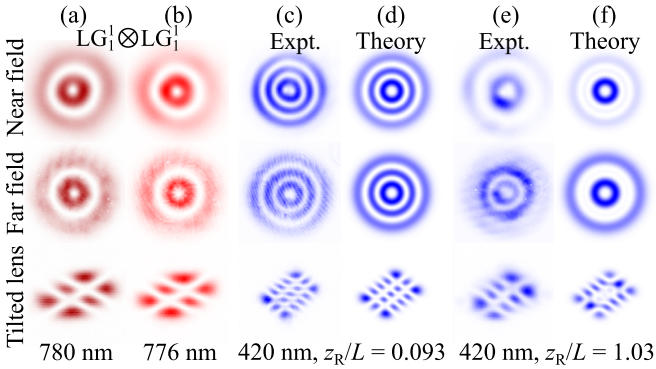

FIG. 4. FWM for both (a) the 780-nm pump and (b) the 776-nm pump in LG_1^1, with image triplets as defined in Fig. 2. (c) For a thick medium we observe the blue light in an almost pure LG_2^2 mode, (d) as predicted. (e) For a thin medium, however, the beam profile changes between the near and far fields, showing less agreement with (f) our simple model.

theoretical model shows some qualitative agreement, but with notable discrepancies, especially in the tilted-lens decomposition. This may indicate that u_{IR} is no longer constrained to the fundamental Gaussian mode or that the Boyd criterion is a poor approximation in this case, as discussed in Sec. S1 of the Supplemental Material [41].

In the remainder of this Letter we work in the thick-medium regime where mode conversion is governed by Gouy phase matching and OAM conversion, as dictated by the 3D mode overlap. In this regime we find excellent agreement with our theoretical model when restricting the unobserved IR beam to $u_{IR} = LG_0^0$. We demonstrate in Fig. 5 the generation of blue light in LG_p^2, where p takes all values from 0 to 8. We achieve this by using pump modes (Supplemental Material [41], Fig. S4) $u_{780} \otimes u_{776} = LG_{p_{780}}^1 \otimes LG_{p_{776}}^1$, with $p_B = p_{780} + p_{776}$. The p index can be identified from the observed intensity profiles as the number of nodal rings. We support this qualitative analysis by showing the associated high-visibility interferograms (Supplemental Material [41], Fig. S5), formed by superposing the blue output beam with its mirror image, allowing us to determine ℓ by azimuthal Fourier decomposition. Even at high p values, the interferograms confirm that $\ell_B = 2$, indicating high-fidelity pump OAM transfer, without increasing the spiral bandwidth, i.e., without spreading the OAM distribution.

In conclusion, we have demonstrated a wide range of mode transformations facilitated by FWM in an atomic vapor, exploring the interplay between radial and azimuthal mode indices. Specifically, we have seen that input beams with $p = 0$ and opposite ℓ values can generate a radial $p = 1$ mode, while FWM light in higher-order radial modes results from "adding" the p values of the input modes. The generated mode decomposition critically depends on the medium thickness. Gouy phase matching plays an increasing role as the length of the medium approaches and exceeds the Rayleigh range, thus limiting the number of participating eigenmodes. Our experiments are consistent, especially in the thick-medium regime, with the assumption that the 5.2-μm light is generated only in the LG_0^0 mode. Interestingly, this cannot be explained by the mode-overlap integrals alone, and a conclusive explanation is still outstanding.

We expect that our results are relevant for nonlinear processes beyond FWM. In the thick-medium limit, possible avenues of research exist both in "macroscopic" nonlinear optics (with crystals and atomic vapors) and in nonlinear photonic waveguides [58,59], which can support LG beam modes [60,61] and where the extreme nonlinearities could lead to highly efficient on-chip wavelength and mode transformations. Most LG communication applications to date have been restricted to the azimuthal mode index, limiting the available information density. The possibility to convert efficiently between radial and azimuthal modes allows access to the full state space for spatial mode encoding, with potential applications in all-optical communication and computing.

In the thin-medium limit [62] we foresee that the addition of high p modes may lead to high "radial bandwidth" entangled photons in much the same way that high ℓ leads to high spiral bandwidth [33,63]; however, correlation strength

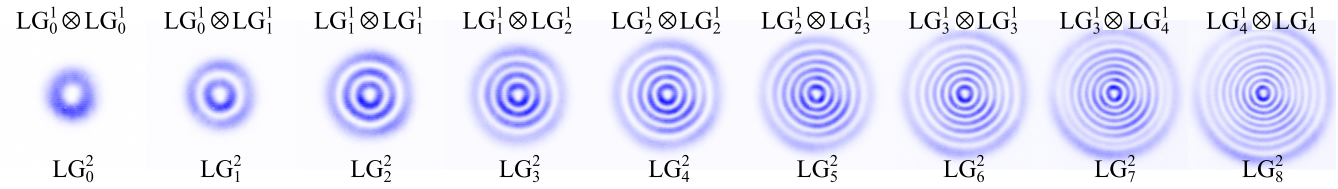

FIG. 5. Generation of higher-order p modes using FWM in the thick-medium regime ($z_R/L = 0.093$). Using a variety of $LG^1_{p780} \otimes LG^1_{p776}$ pump-mode combinations at 780 and 776 nm, we generate blue light in modes with $\ell_B = 2$ and $0 \leqslant p_B \leqslant 8$, shown as near-field peak-normalized profiles.

may depend on the degree of Gouy phase matching. This is interesting both from the perspective of fundamental quantum concepts and due to the increase of the potential state space available for application in optical quantum processes.

There have been exciting recent results on extending resonant atomic four-wave mixing processes, as described in this paper, into the realms of deep-UV, midinfrared, and terahertz (THz) waves [64–66]. Clean mode conversion from the optical into these relatively inaccessible spectral regions, where reconfigurable optical elements like SLMs are not yet readily available, opens new research and development prospects for, e.g., THz imaging [67].

The data set for this paper is available from Ref. [68].

We are grateful for valuable discussions with I. Novikova, as well as for funding via the Leverhulme Trust (Grant No. RPG-2013-386) and EPSRC (Grant No. EP/M506643/1).

[1] L. Allen, M. W. Beijersbergen, R. J. C. Spreeuw, and J. P. Woerdman, Orbital angular momentum of light and the transformation of Laguerre-Gaussian laser modes, Phys. Rev. A **45**, 8185 (1992).

[2] J. Ni, Z. Wang, Z. Li, Z. Lao, Y. Hu, S. Ji, B. Xu, C. Zhang, J. Li, D. Wu, and J. Chu, Multifurcate assembly of slanted micropillars fabricated by superposition of optical vortices and application in high-efficiency trapping microparticles, Adv. Funct. Mater. **27**, 1701939 (2017).

[3] X. Pan, S. Yu, Y. Zhou, K. Zhang, K. Zhang, S. Lv, S. Li, W. Wang, and J. Jing, Orbital-Angular-Momentum Multiplexed Continuous-Variable Entanglement from Four-Wave Mixing in Hot Atomic Vapor, Phys. Rev. Lett. **123**, 070506 (2019).

[4] D.-S. Ding, W. Zhang, S. Shi, Z.-Y. Zhou, Y. Li, B.-S. Shi, and G.-C. Guo, High-dimensional entanglement between distant atomic-ensemble memories, Light Sci. Appl. **5**, e16157 (2016).

[5] G. Gibson, J. Courtial, M. J. Padgett, M. Vasnetsov, V. Pas'ko, S. M. Barnett, and S. Franke-Arnold, Free-space information transfer using light beams carrying orbital angular momentum, Opt. Express **12**, 5448 (2004).

[6] Z. Yue, H. Ren, S. Wei, J. Lin, and M. Gu, Angular-momentum nanometrology in an ultrathin plasmonic topological insulator film, Nat. Commun. **9**, 4413 (2018).

[7] N. Bozinovic, Y. Yue, Y. Ren, M. Tur, P. Kristensen, H. Huang, A. E. Willner, and S. Ramachandran, Terabit-scale orbital angular momentum mode division multiplexing in fibers, Science **340**, 1545 (2013).

[8] A. M. Yao and M. J. Padgett, Orbital angular momentum: Origins, behavior and applications, Adv. Opt. Photonics **3**, 161 (2011).

[9] K. Y. Bliokh, F. J. Rodríguez-Fortuño, F. Nori, and A. V. Zayats, Spin–orbit interactions of light, Nat. Photonics **9**, 796 (2015).

[10] H. Rubinsztein-Dunlop *et al.*, Roadmap on structured light, J. Opt. **19**, 013001 (2016).

[11] S. Franke-Arnold, Optical angular momentum and atoms, Philos. Trans. R. Soc. A **375**, 20150435 (2017).

[12] E. Karimi and E. Santamato, Radial coherent and intelligent states of paraxial wave equation, Opt. Lett. **37**, 2484 (2012).

[13] M. Mazilu, A. Mourka, T. Vettenburg, E. M. Wright, and K. Dholakia, Simultaneous determination of the constituent azimuthal and radial mode indices for light fields possessing orbital angular momentum, Appl. Phys. Lett. **100**, 231115 (2012).

[14] A. Dudley, T. Mhlanga, M. Lavery, A. McDonald, F. S. Roux, M. Padgett, and A. Forbes, Efficient sorting of Bessel beams, Opt. Express **21**, 165 (2013).

[15] J. Zhou, W. Zhang, and L. Chen, Experimental detection of high-order or fractional orbital angular momentum of light based on a robust mode converter, Appl. Phys. Lett. **108**, 111108 (2016).

[16] N. K. Fontaine, R. Ryf, H. Chen, D. T. Neilson, K. Kim, and J. Carpenter, Laguerre-Gaussian mode sorter, Nat. Commun. **10**, 1865 (2019).

[17] Y. Zhou, M. Mirhosseini, D. Fu, J. Zhao, S. M. Hashemi Rafsanjani, A. E. Willner, and R. W. Boyd, Sorting Photons by Radial Quantum Number, Phys. Rev. Lett. **119**, 263602 (2017).

[18] X. Gu, M. Krenn, M. Erhard, and A. Zeilinger, Gouy Phase Radial Mode Sorter for Light: Concepts and Experiments, Phys. Rev. Lett. **120**, 103601 (2018).

[19] V. D. Salakhutdinov, E. R. Eliel, and W. Löffler, Full-Field Quantum Correlations of Spatially Entangled Photons, Phys. Rev. Lett. **108**, 173604 (2012).

[20] E. Karimi, D. Giovannini, E. Bolduc, N. Bent, F. M. Miatto, M. J. Padgett, and R. W. Boyd, Exploring the quantum nature of the radial degree of freedom of a photon via Hong-Ou-Mandel interference, Phys. Rev. A **89**, 013829 (2014).

[21] E. Karimi, R. W. Boyd, P. de la Hoz, H. de Guise, J. Řeháček, Z. Hradil, A. Aiello, G. Leuchs, and L. L. Sánchez-Soto, Radial quantum number of Laguerre-Gauss modes, Phys. Rev. A **89**, 063813 (2014).

[22] W. N. Plick and M. Krenn, Physical meaning of the radial index of Laguerre-Gauss beams, Phys. Rev. A **92**, 063841 (2015).

[23] D. Zhang, X. Qiu, W. Zhang, and L. Chen, Violation of a Bell inequality in two-dimensional state spaces for radial quantum number, Phys. Rev. A **98**, 042134 (2018).

[24] L. Chen, T. Ma, X. Qiu, D. Zhang, W. Zhang, and R. W. Boyd, Realization of the Einstein-Podolsky-Rosen Paradox Using Radial Position and Radial Momentum Variables, Phys. Rev. Lett. **123**, 060403 (2019).

[25] A. M. Yao, Angular momentum decomposition of entangled photons with an arbitrary pump, New J. Phys. **13**, 053048 (2011).

[26] G. H. Shao, Z. J. Wu, J. H. Chen, F. Xu, and Y. Q. Lu, Nonlinear frequency conversion of fields with orbital angular momentum using quasi-phase-matching, Phys. Rev. A **88**, 063827 (2013).

[27] J. Courtial, K. Dholakia, L. Allen, and M. J. Padgett, Second-harmonic generation and the conservation of orbital angular momentum with high-order Laguerre-Gaussian modes, Phys. Rev. A **56**, 4193 (1997).

[28] A. Mair, A. Vaziri, G. Weihs, and A. Zeilinger, Entanglement of the orbital angular momentum states of photons, Nature (London) **412**, 313 (2001).

[29] S. Franke-Arnold, S. M. Barnett, M. J. Padgett, and L. Allen, Two-photon entanglement of orbital angular momentum states, Phys. Rev. A **65**, 033823 (2002).

[30] G. Walker, A. S. Arnold, and S. Franke-Arnold, Trans-spectral Orbital Angular Momentum Transfer via Four-Wave Mixing in Rb Vapor, Phys. Rev. Lett. **108**, 243601 (2012).

[31] A. M. Akulshin, I. Novikova, E. E. Mikhailov, S. A. Suslov, and R. J. McLean, Arithmetic with optical topological charges in stepwise-excited Rb vapor, Opt. Lett. **41**, 1146 (2016).

[32] A. Chopinaud, M. Jacquey, B. Viaris de Lesegno, and L. Pruvost, High helicity vortex conversion in a rubidium vapor, Phys. Rev. A **97**, 063806 (2018).

[33] R. F. Offer, D. Stulga, E. Riis, S. Franke-Arnold, and A. S. Arnold, Spiral bandwidth of four-wave mixing in Rb vapour, Commun. Phys. **1**, 84 (2018).

[34] L. J. Pereira, W. T. Buono, D. S. Tasca, K. Dechoum, and A. Z. Khoury, Orbital-angular-momentum mixing in type-II second-harmonic generation, Phys. Rev. A **96**, 053856 (2017).

[35] G. B. Alves, R. F. Barros, D. S. Tasca, C. E. R. Souza, and A. Z. Khoury, Conditions for optical parametric oscillation with a structured light pump, Phys. Rev. A **98**, 063825 (2018).

[36] B. P. da Silva, D. S. Tasca, E. F. Galvão, and A. Z. Khoury, Astigmatic tomography of orbital-angular-momentum superpositions, Phys. Rev. A **99**, 043820 (2019).

[37] H.-J. Wu, L.-W. Mao, Y.-J. Yang, C. Rosales-Guzmán, W. Gao, B.-S. Shi, and Z.-H. Zhu, Radial modal transitions of Laguerre-Gauss modes during parametric up-conversion: Towards the full-field selection rule of spatial modes, Phys. Rev. A **101**, 063805 (2020).

[38] W. T. Buono, A. Santos, M. R. Maia, L. J. Pereira, D. S. Tasca, K. Dechoum, T. Ruchon, and A. Z. Khoury, Chiral relations and radial-angular coupling in nonlinear interactions of optical vortices, Phys. Rev. A **101**, 043821 (2020).

[39] R.-Z. Zhao, R.-E. Lu, X.-H. Hong, X. Feng, Y.-G. Xu, X.-D. Yuan, C. Zhang, Y.-Q. Qin, and Y.-Y. Zhu, Conversion and manipulation of radial quantum modes in second-harmonic-generation processes, Phys. Rev. A **101**, 023834 (2020).

[40] R. N. Lanning, Z. Xiao, M. Zhang, I. Novikova, E. E. Mikhailov, and J. P. Dowling, Gaussian-beam-propagation theory for nonlinear optics involving an analytical treatment of orbital-angular-momentum transfer, Phys. Rev. A **96**, 013830 (2017).

[41] See Supplemental Material at http://link.aps.org/supplemental/10.1103/PhysRevA.103.L021502 for more details on the theoretical model (S1), experimental details (S2), and supporting results (S3).

[42] G. D. Boyd and D. A. Kleinman, Parametric interaction of focused Gaussian light beams, J. Appl. Phys. **39**, 3597 (1968).

[43] L. Paterson, M. P. MacDonald, J. Arlt, W. Sibbett, P. E. Bryant, and K. Dholakia, Controlled rotation of optically trapped microscopic particles, Science **292**, 912 (2001).

[44] L. Amico, A. Osterloh, and F. Cataliotti, Quantum Many Particle Systems in Ring-Shaped Optical Lattices, Phys. Rev. Lett. **95**, 063201 (2005).

[45] S. Franke-Arnold, J. Leach, M. J. Padgett, V. E. Lembessis, D. Ellinas, A. J. Wright, J. M. Girkin, P. Öhberg, and A. S. Arnold, Optical ferris wheel for ultracold atoms, Opt. Express **15**, 8619 (2007).

[46] M. Bhattacharya, Lattice with a twist: Helical waveguides for ultracold matter, Opt. Commun. **279**, 219 (2007).

[47] A. S. Arnold, Extending dark optical trapping geometries, Opt. Lett. **37**, 2505 (2012).

[48] S. N. Alperin, R. D. Niederriter, J. T. Gopinath, and M. E. Siemens, Quantitative measurement of the orbital angular momentum of light with a single, stationary lens, Opt. Lett. **41**, 5019 (2016).

[49] A. S. Zibrov, M. D. Lukin, L. Hollberg, and M. O. Scully, Efficient frequency up-conversion in resonant coherent media, Phys. Rev. A **65**, 051801(R) (2002).

[50] T. Meijer, J. D. White, B. Smeets, M. Jeppesen, and R. E. Scholten, Blue five-level frequency-upconversion system in rubidium, Opt. Lett. **31**, 1002 (2006).

[51] J. T. Schultz, S. Abend, D. Döring, J. E. Debs, P. A. Altin, J. D. White, N. P. Robins, and J. D. Close, Coherent 455 nm beam production in a cesium vapor, Opt. Lett. **34**, 2321 (2009).

[52] A. M. Akulshin, R. J. McLean, A. I. Sidorov, and P. Hannaford, Coherent and collimated blue light generated by four-wave mixing in Rb vapour, Opt. Express **17**, 22861 (2009).

[53] A. Vernier, S. Franke-Arnold, E. Riis, and A. S. Arnold, Enhanced frequency up-conversion in Rb vapor, Opt. Express **18**, 17020 (2010).

[54] R. F. Offer, J. W. C. Conway, E. Riis, S. Franke-Arnold, and A. S. Arnold, Cavity-enhanced frequency up-conversion in rubidium vapor, Opt. Lett. **41**, 2177 (2016).

[55] E. Brekke and S. Potier, Optical cavity for enhanced parametric four-wave mixing in rubidium, Appl. Opt. **56**, 46 (2017).

[56] A. S. Arnold, J. S. Wilson, and M. G. Boshier, A simple extended-cavity diode laser, Rev. Sci. Instrum. **69**, 1236 (1998).

[57] T. W. Clark, R. F. Offer, S. Franke-Arnold, A. S. Arnold, and N. Radwell, Comparison of beam generation techniques using a phase only spatial light modulator, Opt. Express **24**, 6249 (2016).

[58] J. Wang, F. Sciarrino, A. Laing, and M. G. Thompson, Integrated photonic quantum technologies, Nat. Photonics **14**, 273 (2019).

[59] J.-H. Kim, S. Aghaeimeibodi, J. Carolan, D. Englund, and E. Waks, Hybrid integration methods for on-chip quantum photonics, Optica **7**, 291 (2020).

[60] Y. Chen, J. Gao, Z.-Q. Jiao, K. Sun, W.-G. Shen, L.-F. Qiao, H. Tang, X.-F. Lin, and X.-M. Jin, Mapping Twisted Light into and out of a Photonic Chip, Phys. Rev. Lett. **121**, 233602 (2018).

[61] Y. Chen, K.-Y. Xia, W.-G. Shen, J. Gao, Z.-Q. Yan, Z.-Q. Jiao, J.-P. Dou, H. Tang, Y.-Q. Lu, and X.-M. Jin, Vector Vortex Beam Emitter Embedded in a Photonic Chip, Phys. Rev. Lett. **124**, 153601 (2020).

[62] T. F. Cutler, W. J. Hamlyn, J. Renger, K. A. Whittaker, D. Pizzey, I. G. Hughes, V. Sandoghdar, and C. S. Adams, Nanostructured Alkali-Metal Vapor Cells, Phys. Rev. Appl. **14**, 034054 (2020).

[63] D.-S. Ding, M.-X. Dong, W. Zhang, S. Shi, Y.-C. Yu, Y.-H. Ye, G.-C. Guo, and B.-S. Shi, Broad spiral bandwidth of orbital angular momentum interface between photon and memory, Commun. Phys. **2**, 100 (2019).

[64] D. Antypas, O. Tretiak, D. Budker, and A. Akulshin, Polychromatic, continuous-wave mirrorless lasing from monochromatic pumping of cesium vapor, Opt. Lett. **44**, 3657 (2019).

[65] M. Lam, S. B. Pal, T. Vogt, C. Gross, M. Kiffner, and W. Li, Collimated UV light generation by two-photon excitation to a Rydberg state in Rb vapor, Opt. Lett. **44**, 2931 (2019).

[66] M. Lam, S. B. Pal, T. Vogt, M. Kiffner, and W. Li, Directional THz generation in hot Rb vapor excited to a Rydberg state, Opt. Lett. **46**, 1017 (2021).

[67] L. A. Downes, A. R. MacKellar, D. J. Whiting, C. Bourgenot, C. S. Adams, and K. J. Weatherill, Full-Field Terahertz Imaging at Kilohertz Frame Rates Using Atomic Vapor, Phys. Rev. X **10**, 011027 (2020).

[68] Dataset at: https://doi.org/10.15129/578985d6-ff89-4be9-aa78-8710aeeac92d.